Atmos. Chem. Phys. Discuss., 8, 20239–20281, 2008
www.atmos-chem-phys-discuss.net/8/20239/2008/

Atmospheric Chemistry and Physics Discussions

This discussion paper is/has been under review for the journal *Atmospheric Chemistry and Physics (ACP)*. Please refer to the corresponding final paper in *ACP* if available.

Mechanisms controlling surface ozone over East Asia: a multiscale study coupling regional and global chemical transport models

M. Lin[1], T. Holloway[1], T. Oki[2], D. G. Streets[3], and A. Richter[4]

[1]Center for Sustainability and the Global Environment (SAGE), University of Wisconsin-Madison, Madison, WI, USA
[2]Institute of Industrial Science, University of Tokyo, Tokyo, Japan
[3]Argonne National Laboratory, Argonne, IL, USA
[4]Institute of Environmental Physics, University of Bremen, Bremen, Germany

Received: 18 August 2008 – Accepted: 3 October 2008 – Published: 3 December 2008

Correspondence to: M. Lin (mlin26@wisc.edu)

Published by Copernicus Publications on behalf of the European Geosciences Union.

Abstract

Mechanisms controlling surface ozone (O_3) over East Asia are examined using the regional Community Multiscale Air Quality (CMAQ) model at two horizontal scales: 81 km and 27 km. Through sensitivity studies and comparison with recently available satellite data and surface measurements in China and Japan, we find that the O_3 budget over East Asia shows complex interactions among photochemical production, regional transport, meteorological conditions, burning of agricultural residues, and global inflows. For example, wintertime surface O_3 over northern domain is sensitive to boundary conditions derived from the MOZART (Model for Ozone and Related Tracers) global model, whereas summertime O_3 budget is controlled by the competitive processes between photochemical production and monsoonal intrusion of low-O_3 marine air masses from tropical Pacific. We find that simulated surface O_3 for 2001 does not exhibit the same sharp drop in July and August concentrations that is observed at two mountaintop sites (Tai and Hua) for 2004 and Beijing for 1995–2005. CMAQ sensitivity tests with two widely used photochemical schemes demonstrate that over the industrial areas in East Asia north of 30° N, SAPRC99 produces higher values of mean summertime O_3 than CBIV, amounting to a difference of 10 ppb. In addition, analysis of NCEP winds and geopotential heights suggests that southwesterly monsoonal intrusion in central east China is weakened in August 2001 as compared with the climatologically mean for 1980–2005. Further examination of the O_3 diurnal cycle at nine Japanese sites shows that boundary layer evolution has an important effect on the vertical mixing of ground-level O_3, and error in near surface meteorology might contribute to overprediction of nighttime O_3 in urban and rural areas. In conclusion, the uncertainties in simulating cloud activities and convection mixing, Asian monsoon circulation, photochemical production, and nighttime cooling explain why CMAQ with 81 km horizontal scale overpredicts the observed surface O_3 in July and August over central east China and central Japan by 5–15 ppb (CBIV) and 15–25 ppb (SAPRC99). The results suggest clear benefits in evaluating atmospheric chemistry over Asia with high resolution

ACPD

8, 20239–20281, 2008

regional model.

1 Introduction

Ozone (O_3) is a secondary pollutant produced in the troposphere by photochemical oxidation of non-methane volatile organic compounds (NMVOCs), carbon monoxide (CO), and methane (Fiore et al., 2002) in the presence of nitrogen oxides (NO_x=NO+NO_2) radicals. Ground-level O_3 is a major ingredient of urban smog that poses a significant risk for public health, and O_3 throughout the troposphere is an important greenhouse gas (Fishman et al., 1979). Ozonesonde observations in Japan (Naja and Akimoto, 2004) and Hong Kong (Liu et al., 2002) show that the seasonal cycle of O_3 in the boundary layer has a broad summer minimum at low latitudes of the Asian Pacific Rim, in contrast to summer maximum observed at regionally polluted sites in North America and Europe (Jacob, 1999). Recent studies over eastern China report that surface O_3 exhibits a narrow peak in early summer (May or June) and a sharp drop in July and August, based on measurements taken in Beijing (Ding et al., 2008; Lin et al., 2008c), at three mountaintop sites (Li et al., 2007), and at the rural site Lin'an (Xu et al., 2008). However, a distinctly different seasonal pattern of surface O_3 with a broad summertime maximum during May–August is observed at Mt. Waliguan, which is located in the northeastern edge of the Tibetan Plateau. Meteorological simulations (Ding and Wang, 2006) and regional model analysis by tagging emission sources (Ma et al., 2002, 2005) suggest that the elevated surface O_3 concentrations at Waliguan are mostly caused by the downward transport of stratospheric air, as opposed to transport of anthropogenic pollutions from eastern China (Zhu et al., 2004). Other sources affecting Asia include European emissions, which exert the strongest influence on lower troposphere O_3 in East Asia in the springtime, and North American emissions which exhibit the greatest influence in the upper troposphere, in the fall (Wild et al., 2004; Liu et al., 2002; Holloway et al., 2007).

Accurate prediction of tropospheric O_3 presents a particular challenge in chemical

ACPD
8, 20239–20281, 2008

transport models (CTMs) due to the complex physical and chemical processes occurring from global to local scales and by their strong coupling across scales. A number of regional CTMs have been applied to study episodic chemical transport and transformation of Asian pollutants in springtime (e.g. Carmichael et al., 2003b; Zhang et al., 2003; Wang et al., 2006b), and the seasonal cycle of surface O_3 in eastern China (Li et al., 2007) and Japan (Yamaji et al., 2006). Results from MICS-Asia regional model intercomparison found that O_3 predictions for July over central east China differ by ~20 ppb among seven regional CTMs (Han et al., 2007). This divergence in model estimates suggests that important questions remain on the key mechanisms controlling the O_3 budget over East Asia. The chemical mechanisms have been found to substantially impact model predictions and sensitivity to NMVOCs and NO_x emission controls over North America (e.g., Sarwar et al., 2008; Luecken et al., 2007; Arnold and Dennis, 2006). However, the response of local and regional O_3 in Asia to choice and implementation of chemical mechanisms has not yet been evaluated.

This study employs the regional Community Multiscale Air Quality (CMAQ v. 4.5.1) model (Byun and Ching, 1999; Byun and Schere, 2006) and the global Model for Ozone and Related Tracers (MOZART v. 2.4) (Horowitz et al., 2003) to examine mechanisms controlling surface O_3 over East Asia, including the impacts of boundary conditions (BCs), photochemical schemes, long-range transport, agricultural burning, and meteorological conditions. Section 2 gives an overview of observational data of ground-based stations and satellite remote sensing, regional and global models used, BCs treatment, and chemical mechanisms. Discussion on O_3 seasonality is presented in Sect. 3. We first examine the impacts of both global model BCs and photochemistry on seasonal predictions of surface O_3 at available ground-based measurements in Siberia, Japan, China, and Southeast Asia. Then with a focus on the summer season, O_3 production efficiency and spatial variability are analyzed in detail as they respond to different chemical schemes. Satellite data of tropospheric NO_2 columns and fire count are used to discuss the impacts of agricultural burning over central east China. Influence of long-range transport are also evaluated. Section 4 examines diurnal variability of sum-

ACPD
8, 20239–20281, 2008

mertime ground-level O_3. Discussion includes the sensitivity of model resolution and time-varying BCs, and the correlation with NO_x concentrations, boundary layer height, and surface wind speed.

2 Models and data

2.1 Observational data

Surface measurement data for O_3 and NO_x in Japan obtained under the EANET (Acid Deposition Monitoring Network in Asia) monitoring program (EANET, 2002) were made available for this study. Compared with Japan, there are few long-term measurement sites for O_3 in China. To help validate the simulated seasonal cycle of surface O_3 in China and Southeast Asia, we collected measurement data from recently published research papers (Table 1). Locations of measurement sites are shown in Fig. 1. It should be noted that measurement data collected from different research papers might not be in the same year as the 2001 model simulations. In Sect. 3.3, we have discussed inter-annual variability of meteorological conditions and associated impact on O_3 concentrations.

Satellite data of tropospheric NO_2 columns and fire count are used to help interpret the discrepancies between modeled and observed seasonal variations of surface O_3. Tropospheric NO_2 column (monthly mean, $0.25\times0.25^{\circ}$) is based on the GOME (Global Ozone Monitoring Experiment) retrieval by Bremen University (Richter et al., 2005). CMAQ results are sampled at the GOME overpass time at China to calculate tropospheric NO_2 column (Lin et al., 2008b). To examine the intensity of biomass burning and its impact on O_3 concentrations, we use the total fire count maps from MODIS (Moderate Resolution Imaging Spectroradiometer) on NASA's Aqua satellite. The MODIS data is obtained from Louisa Emmons at NCAR (National Center for Atmospheric Research).

ACPD
8, 20239–20281, 2008

2.2 Model configurations

To distinguish mechanisms controlling surface O_3 over East Asia from regional to local scale, the CMAQ model is employed at two horizontal scales, an $81 \times 81\,km^2$ primary domain over East Asia and a $27 \times 27\,km^2$ nested domain over Northeast Asia (Fig. 2a). The fine domain covers eastern China, the Korean Peninsula and Japan, and is designed to avoid crossing strong local sources at the boundaries. The meteorological fields for both domains are generated from the MM5 meteorological model (Grell et al., 1994) driven with NCEP/NCAR $2.5 \times 2.5^\circ$ global reanalysis data every six hours for 2001. The MM5 simulations apply the three-dimensional grid nudging technique and include 23 vertical layers with the depth of first layer setting to 73 m. Vertical layer collapsing is performed to generate eight-layer meteorological fields for CMAQ. We have tested CMAQ with a full range of 23 vertical layers and the results show that the vertical layer collapsing does not significantly undermine CMAQ performance. The cloud scheme of Grell et al. (1994) was chosen for the physical parameterization, and the MRF (Medium Range Forecast) scheme of Hong and Pan (1996) was employed for PBL (planetary boundary layer) parameterization.

We have employed the same models to study long-range transport and fate of acidifying substances over East Asia, and the results are presented in Lin et al. (2008b) for model evaluation and in Lin et al. (2008a) for estimating source-receptor relationships. The reader is referred to Lin et al. (2008b) for a detail description of MM5 simulations, emission data and their processing. With mostly same model configurations as described in Lin et al. (2008b), which focuses on acidifying substances, the present study focuses on O_3 and associated chemistry and physics. Additional model treatments are described in Sect. 2.3 for gas-phase chemistry and in Sect. 2.4 for boundary conditions.

Monthly mean NCEP/NCAR winds and geopotential heights during 1980–2005 are used to demonstrate the climatological features of East Asian summer monsoon circulation. In addition, to evaluate the influence of long-range transport on summertime O_3 budget, we calculated three-day back-trajectories using HYSPLIT (HYbrid Single- Par-

ACPD
8, 20239–20281, 2008

ticle Lagrangian Integrated Trajectory, version 4.8) model of NOAA Air Resources Laboratory (http://www.arl.noaa.gov/ready/hysplit4.html). The HYSPLIT model was driven with the formated Final Analysis data (FNL) which has a horizontal resolution of approximately 190 km, 13 vertical layers and 6-h temporal resolution.

2.3 Gas phase chemistry

In the interest of evaluating model sensitivities to photochemical schemes, we have tested two widely used chemical mechanisms, the Carbon Bond IV (CBIV) mechanism (Gery et al., 1989) and the Statewide Air Pollution Research Center (SAPRC99) mechanism (Carter, 2000). The speciation of NMVOCs to the mechanism-dependent species of CBIV and SAPRC99 is based on a new emission processing model as described in Lin et al. (2008b). CBIV is a lumped-structure condensed mechanism in which organic species are categorized according to the reactions of similar carbon bonds (C–C, C=C, C–CHO etc.). The CBIV mechanism in CMAQ contains 36 species and 93 reactions including 11 photolytic reactions. Compared with CBIV, SAPRC99 includes more detailed organic chemistry, explicit organic peroxy radicals, and more complete organic intermediates, and provides better representation of peroxides for low NO_x conditions. The SAPRC99 mechanism has assignments for 400 types of VOCs, and can be used to estimate reactivities for 550 VOC categories (Carter, 2000). A total of 24 model species are used to represent the reactive organic product species: 11 are explicit, and 13 represent groups of similar oxidation reactivity and emission magnitudes using the lumped molecule approach. The SAPRC99 mechanism in CMAQ includes 72 species and 214 reactions including 30 photolytic reactions.

2.4 Boundary conditions

In addition to chemistry, treatment of lateral and top boundary conditions (BCs) is another major factor affecting regional CTM predictions, especially for long-lived species such as O_3, PAN (peroxyacetyl nitrate), and CO etc. To examine the impacts of BCs,

ACPD
8, 20239–20281, 2008

we have tested several options, including monthly mean original and measurement-adjusted global model BCs, and hourly varying BCs from the coarse CMAQ simulation.

Compared with lateral-fixed BC derived from in-situ measurements, the global model BC provides more realistic spatial and temporal variability. Global CTMs, however, are themselves uncertain, so using global model BCs might introduce additional uncertainty to regional model predictions (Tang et al., 2007). In this study, the CMAQ 81 km predictions used monthly mean BCs derived from the MOZART global model. The simulation of the global MOZART model is driven with NCEP reanalysis meteorology for 2000–2002 (hereafter referred to as MOZART-NCEP). The evaluation by Holloway et al. (2007) showed that MOZART-NCEP tends to overpredict monthly averaged EANET surface O_3 over Japan except in springtime. The overprediction is particularly significant, up to 40%, in summertime. In order to reduce the uncertainties introduced in the import of MOZART-derived BCs, we adjusted the concentration of O_3 at the domain boundaries to correct for the MOZART bias over Japan as evaluated in Holloway et al. (2007). The percentage adjustments, which vary on monthly basis from 0 to 40%, are plotted in Fig. 2a. Results of the CMAQ predictions with original and adjusted MOZART BCs are presented in Sect. 3.1.

Monthly mean BCs provide a seasonal perspective, but do not resolve possible episodic signals. Thus, we drive the CMAQ 27 km prediction with hourly varying BCs extracted from the CMAQ 81 km simulation to see how temporal variation of BCs influences predicted O_3. The results are presented in Sect. 4.

3 Seasonal cycle of surface ozone

We performed three CMAQ regional simulations at 81 km horizontal scale with different chemical mechanisms and global BCs, and compared seasonal variations of surface O_3 predictions with ground-based measurements. Measurement sites are classified into three groups representing different seasonal patterns at higher latitudes (Fig. 2a), lower latitudes (Fig. 2b) and mid-latitudes (Figs. 2c and 3) in the study domain. Corre-

ACPD
8, 20239–20281, 2008

lation coefficient (R), mean bias (MB), and root mean square error ($RMSE$) are chosen to measure the model performance.

3.1 Impacts of boundary conditions

Three ground-based measurement sites (Mondy, Rishiri, and Tappi) close to the northern boundary of the study domain (Fig. 2a) are chosen to diagnose the impacts of MOZART BCs. The comparison between two SAPRC99 predictions with original and adjusted MOZART BCs demonstrates that adjusting MOZART BCs of O_3 reduces the mean bias by ~5 ppb on seasonal predictions at these three sites. CMAQ predictions at Mondy with adjusted O_3 BC show correlations of R=0.92 as contrast to R=0.73 with original MOZART BCs. Adjusting the MOZART-derived O_3 BCs exerts a greater influence on wintertime O_3 predictions, indicating longer lifetime of O_3 in the wintertime atmosphere. Using measurement-adjusted O_3 BCs tends to improve CMAQ performance in predicting wintertime surface O_3 in northern (Rishiri and Tappi) and central Japan (Oki) as compared with measurements.

3.2 Impacts of chemical schemes

Comparison of CMAQ simulations with two widely-used chemical schemes shows that the difference in surface O_3 predictions between CBIV and SAPRC99 is negligible in wintertime, but amounts for ~10 ppb difference in summertime. The divergence of summertime O_3 predictions between two chemical schemes is particularly pronounced at regionally polluted or downwind sites in mid-latitudes (Figs. 2c and 3). In contrast, photochemistry exerts a much smaller influence at coastal and island sites in lower latitudes of the Asian Pacific Rim (Fig. 2b). The high chemical sensitivity in the polluted regions and in downwind areas reflects the fact that the summertime O_3 budget is dominated by local processes of NO_x-NMVOC-CO photochemistry. Our results over East Asia show that for O_3, SAPRC99 produces higher values than CBIV, as found over the United States (Arnold and Dennis, 2006; Faraji et al., 2008; Luecken et al.,

ACPD
8, 20239–20281, 2008

2007; Byun, 2002; Yarwood et al., 2003), but while all of these prior studies have focused on O_3 yields at polluted urban sites. We show the same tendencies at remote coastal sites (Oki, Tappi, and Rishiri), reflecting the influence of northeasterly transport in the boundary layer in Northeast Asia summertime (see Fig. 4). We find that both CBIV and SAPRC99 tend to overpredict summertime O_3 at mid-latitudes sites, but the overprediction by SAPRC99 is more significant. CMAQ with the CBIV chemistry better captures both the seasonal variations and magnitudes of observed monthly mean O_3 at most sites shown in Figs. 2 and 3. The SAPRC99 chemistry, however, overpredicts summertime surface O_3 by 15–25 ppb at the mountainous sites (Mt. Tai and Mt. Hua) and the coastal sites (Oki and Pohang).

To further examine the spatial variations of chemical sensitivities, Fig. 4 shows the distributions of monthly mean surface O_3 and peroxyacetyl nitrate (PAN) in July from the SAPRC99 and CBIV predictions. Both simulations show a similar spatial pattern of surface O_3 with low concentrations at south of 30° N and with a region of O_3 in the excess of 45 ppb stretching across Northern China. Central east China and downwind areas show typical concentrations of 60 ppb or higher. The difference between SAPRC99 and CBIV in predicting O_3 is most pronounced in the region between 30° N and 50° N of the study domain. The SAPRC99 mechanism shows a higher O_3 production efficiency over this polluted region where photochemical formation of O_3 tends to dominate the O_3 budget.

Several reasons may explain the higher O_3 predicted by SAPRC99. From the emissions point of view, SAPRC99 includes a more-detailed emission representation of hydrocarbon classification for individual VOC species. Formation of O_3 is thus sensitive to the aggregated emissions of highly reactive VOC species. Emission speciation of VOCs, however, may not take a full advantage of detailed VOC categories by SAPRC99 since most VOC speciation profiles for Asia are based on the source measurements in North America or Europe. In addition to the expected uncertainty in VOC speciation of anthropogenic sources, natural sources of reactive VOCs (especially isoprene and monoterpenes) are poorly known. Isoprene emission, primarily from oaks

ACPD
8, 20239–20281, 2008

and other deciduous trees, exhibits strong seasonal and diurnal variability, depending on the driving variables which include temperature, solar radiation, Leaf Area Index and plant functional type. Biogenic isoprene plays an important role in contributing the summertime O_3 budget in many areas. A sensitivity test of CMAQ with SAPRC99 is carried out by removing biogenic isoprene emissions, and we find that surface O_3 concentrations over central east China and downwind areas decrease by 10–15 ppb in average. The SAPRC99's overprediction of summertime O_3 is likely related to the uncertainty in estimating natural isoprene flux. Online calculation of isoprene emission depending on meteorological conditions is recommended for future studies.

From the chemistry point of view, SAPRC99 is a more reactive mechanism that includes explicit organic peroxy radicals and isoprene chemistry. As shown in Fig. 4, SAPRC99 produces 50–70% more PAN relative to CBIV over polluted central east China. Gas-phase PAN is produced via the reversible reaction of the peroxyacetyl radical with NO_2:$CH_3C(O)OO+NO_2 \rightleftharpoons CH_3C(O)OONO_2$. PAN serves as a reservoir and carrier of NO_x in upper troposphere, and it may be transported over long distances and lead to enhanced O_3 production away from the primary NO_x sources by releasing NO_2 when the air masses warm up (Glatthor et al., 2007). Instead of producing PAN, CBIV produces 10–30% higher nitric acid (HNO_3) which is quickly dry deposited and thus permanently removes a significant fraction of NO_x from the system which otherwise may have been recycled. In addition to the difference in O_3, PAN, and HNO_3 predictions, the two mechanisms also show large differences in formaldehyde (HCHO) and hydrogen peroxide (H_2O_2) concentrations. Photolysis of HCHO can be a significant radical source as well as an important sink of reactive free radicals, so it plays an important role in O_3 chemistry in the troposphere. CMAQ with the SAPRC99 mechanism predicts 10–50% higher HCHO and 20–50% lower H_2O_2 over central east China and downwind areas than CMAQ with the CBIV chemistry.

Compared with monthly mean available O_3 measurements at sites across east Asia (shown as filled circles in Fig. 4), CMAQ shows correlations of R=0.7 (CBIV) and 0.6 (SAPRC99), and root mean square errors of $RMSE$=9.0 ppb (CBIV) and 14.6 ppb

ACPD
8, 20239–20281, 2008

(SAPRC99). Although SAPRC99 includes a more detailed organic chemistry, the results presented here reveal that CMAQ with the CBIV mechanism tends to improve model performance in reproducing observed monthly mean values of ground-level O_3 in China and Japan. The analysis of photochemical sensitivity has demonstrated that the uncertainty in gas-phase chemistry can lead to significant bias for summertime O_3 predictions in the industrial areas of East Asia. SAPRC99 and CBIV response differently to NO_x emissions control. Thus choosing a mechanism that best represents regional atmospheric conditions is essential in regulatory applications,i.e., emissions control policy over central east China.

3.3 Impact of monsoonal intrusion on summertime O_3

The intrusion of low-O_3 marine air masses is the key mechanism contributing to the summer minimum of surface O_3 at the Asian Pacific Rim (Naja and Akimoto, 2004; Liu et al., 2002). As shown in Fig. 2b, the monsoonal summer minimum is more pronounced at lower latitude sites. Surface O_3 at Mt. Sto.Tomos stays as low as 20–30 ppb all year long with weak seasonal variability, indicating seasonal dominance of low emissions sources and marine air masses. At Hedo and Ogasawara, slightly to north, surface O_3 exhibits strong seasonal variations with a maximum in winter and spring, transported from the continental Asia, and a minimum in summer due to southwesterly monsoonal intrusion. The impacts of monsoonal intrusion on O_3 concentrations at three island sites on lower latitudes (Mt. Sto.Tomos, Hedo, and Ogasawara) are reasonably well simulated by the model. All simulations successfully reproduce the observed seasonal cycle of surface O_3 at Hedo with correlation of $R \geq 0.95$. The models also show a correlation of $R=0.8$ at Ogasawara although there is overprediction during January to February likely attributed to the error of MOZART global BCs at the east side.

Compared with the remote island sites, O_3 sources at Chinese sites show more complex interactions among local photochemical production as explained by high chemical sensitivity (Sect. 3.1), transport of regional pollution, and monsoonal intrusion. At the

rural site Lin'an and at three mountaintop sites Huang, Tai and Hua, the observed surface O_3 exhibits a late spring/early summer maximum and drops to low values in July and August. Compared with the observed seasonal trend of surface O_3 in eastern China, the model shows correlations of R=0.54 at Lin'an, R=0.45 at Mt. Huang, R=0.68 at Mt. Tai, and R=0.68 at Mt. Hua. The observed peak in late spring and sharp drop in July of surface O_3 at Lin'an and Mt. Huang are well reproduced by the model, but surface O_3 in August at all eastern China sites are overpredicted. Especially at Mt. Tai, Mt. Hua and Beijing, model simulations with both gas phase chemistry of CBIV and SAPRC99 do not capture the decreasing trend of observed O_3 during summer months of June, July and August.

Overall, CMAQ tends to overpredict surface O_3 in July and August at the mid-latitudes sites in central Japan and central east China (Figs. 2c and 3), consistent with results reported for seven regional CTMs (Han et al., 2007) and 21 global CTMs (Fiore et al., 2008) in comparing with EANET data taken in Japan. The systematic summertime overprediction found in both regional and global CTMs is likely due to model inability in simulating cloud activity and convective mixing, and inadequate representation of southwesterly inflow of marine air masses in the global meteorological analysis data.

It should be noted that model results are for 2001 while measurement data at three mountaintop sites (Mt. Tai, Mt. Hua, and Mt. Huang) obtained from Li et al. (2007) are for March 2004 – February 2005, and aircraft observation over Beijing from Ding et al. (2008) gives the climatological mean during 1995–2005. Wang et al. (2006a) reported approximately 60 ppb of surface O_3 observed in a mountaineous area (40.35° N, 116.30° E) 50 km north of the center of Beijing during 20 June – 31 July 2005. As compared in Fig. 3, the reported measurement for July 2005 is much higher than the mean value in July duing 1995–2005, suggesting large inter-annual variability of summertime O_3 concentrations over Beijing. To examine if there are large inter-annual variations of meteorological conditions which might affect the increased O_3 concentrations in August 2001 over central east China as simulated by the model, we also analyze NCEP/NCAR

ACPD
8, 20239–20281, 2008

winds and geopotential heights at 850 hPa. To provide a climatological perspective of East Asian Summer Monsoon (EASM), we averaged NCEP/NCAR winds and geopotential heights at 850 hPa in June and August over 1980–2005. Figure 5 compares the climatological patterns with those for 2001. Winds and geopotential heights for 2004 show similar patterns to the climatological mean, thus the maps are not shown here. The Western North Pacific (WNP) anticyclone plays an important role in the connection between the EASM and the tropical SST anomalies (e.g. Lee et al., 2008), and is characterized by southwesterly airflow along the east Asian coast. The monsoonal flow transports Asian O_3 pollution along the Pacific Rim towards the northeast, and the pollution episodes are then subject to frequent lifting into the upper troposphere by convection (Liu et al., 2002). As seen from the distribution of geopotential heights for 1980–2005, the monsoon band shifts to northwest in August. Central east China is thus subject to more frequent cloudy and rainy weather in August as contrast to June (Ding et al., 2008), whereas central and south Japan is under weakened monsoon conditions in August. The more frequent impacts of monsoonal air masses from western Pacific to central east China could partially explain the low O_3 observed in August at the eastern China sites, including Mt. Tai and Hua measurements for 2004 (Fig. 2c), Beijing aircraft observatory during 1995–2005 (Fig. 3) (Ding et al., 2008), and ground-based measurement at Shangdianzi near Beijing during 2004–2006 (Lin et al., 2008c).

In 2001, however, we found that the Western North Pacific (WNP) anticyclone moved to the northeast in August as compared with the climatological pattern. The northeastward shift of WNP anticyclone in August 2001 results in relatively less southwesterly monsoonal airflow to central east China and partially contributes the increased O_3 concentration simulated for August 2001. The geopotential heights in Fig. 5 show that there is a localized high pressure system over central east China in August 2001. The relatively high geopotential heights over central east China suggests the weakened EASM in the same region. Supporting this conclusion, comparison of two NCEP precipitation fields shows that the precipitation amount over central east China in August 2001 is

2 mm/day in average lower than that in August of 2004 and the climatological mean.

To examine the influence of long-range transport, 3-day backward trajectories arriving at 1000 m above ground level over Mt. Tai were computed every 6 h (at 00:00, 06:00, 12:00, and 18:00 UT) for August 2001 and August 2004 using the NOAA HYSPLIT 4 model. Cluster analysis was applied to all trajectories in August and the results are shown in Fig. 6. We found that air masses originated from polluted North China Plain (NCP) exerts a stronger influence at Mt. Tai in August 2001 as contrast to August 2004. As shown in Fig. 4 of O_3 distribution map in July, summertime O_3 concentrations in NCP are much higher than that in southern China where frequent impacts of marine air masses occur. Thus more long-range transport of O_3 pollution from NCP also contributes to the discrepancies between model results for 2001 and the measurement at Mt. Tai for 2004.

In summary, the large discrepancy of summertime O_3 between model simulations and measurements for central east China are also attributed to the high uncertainty in photochemical production, the weakened EASM in 2001, and relatively more long-range transport from NCP. In addition, we find that CMAQ overpredicts nighttime O_3 mixing ratios at Beijing by 10–20 ppb as compared with the values reported by measurements (Wang et al., 2006a; Lin et al., 2008c; Ding et al., 2008). CMAQ was initially developed for regulatory purposes, for which daytime O_3 is the greatest concern. Thus the nighttime cooling and vertical mixing physics might not be well parameterized as suggested by previous CMAQ evaluations (e.g. Zhang et al., 2006; Arnold and Dennis, 2006).

3.4 Impacts of agricultural burning in central east China

Comparison of observed and simulated seasonal cycle of surface O_3 at Mt. Tai and Mt. Hua (Fig. 2c) illustrates that CMAQ with the CBIV chemistry underestimates the peak values in June. To examine if there are additional emissions sources in June missing in the model, we compared the CMAQ-derived tropospheric NO_2 columns with the retrieval values from GOME. Figure 7 shows that the magnitude and distribution

ACPD
8, 20239–20281, 2008

of GOME NO_2 in July and August are reasonably reproduced in the model using anthropogenic emissions data from Streets et al. (2003), suggesting the overprediction of O_3 in central east China in July and August is not due to the errors of NO_x emissions. In June, however, we find that strong NO_2 sources over central east China from the GOME retrieval are missing in the CMAQ derived values. We have also examined NO_2 satellite data from more recent instruments (SCIAMACHY, GOME-2, and OMI) and found similar pattern in other years with greater June NO_2 over central east China. The stronger signal of June NO_2 columns from satellites could be attributed to longer lifetime of NO_x compared with rainy/cloudy July and August, and also to additional sources from agricultural burning after harvest in central east China. The MODIS total fire count maps depict that intensive biomass burning activities occurred in June 2001 (Fig. 8), which partially explains the additional NO_2 sources in June from GOME. Distinct differences between June and August MODIS fire count maps over central east China are consistent with ATSR-2 (Along Track Scanning Radiometer 2) total fire count maps (http://dup.esrin.esa.int/ionia/about_ionia.asp).

The present study uses biomass burning emission data for 2000 from GEIA/RETRO database (http://www.aero.jussieu.fr/projet/ACCENT/RETRO.php) because the data for 2001 with seasonal variability was not available when our study was initialized in 2005. In recent years, a more advanced database called GFED (Global Fire Emission Database) with an inter-annual variability during 1997–2006 (van der Werf et al., 2006) has been developed. We find that GFED data for June 2001 reports even more intensive biomass burning emissions as compared with both GEIA/RETRO 2000 (used here) and GFED 2000 (highlighting inter-annual variability) estimates. However, GFED 2001 shows similar magnitude to GFED emissions for June 2004 when the measurements at Mt. Tai and Mt. Hua took place. In addition to the uncertainty in O_3 production rate in the CBIV chemistry, the lack of agricultural burning emissions in June in the model would partially explain why the magnitude of O_3 peak values in June is underestimated by CMAQ with CBIV.

ACPD
8, 20239–20281, 2008

4 Diurnal variability of ground-level ozone

Previous studies examining the budget of tropospheric O_3 along the Asian Pacific Rim (e.g. Liu et al., 2002; Yamaji et al., 2006) generally used monthly or daily mean data. Here, we use hourly data to examine the role of vertical mixing and chemistry evolution on the diurnal features of ground-level O_3. Four sets of O_3 predictions with different chemical schemes of CBIV and SAPRC99, horizontal resolutions of 81 km and 27 km, and boundary conditions of monthly mean and hour varying values are compared with the measurement data at the EANET sites located in Japan (Figs. 9∼10). The observed and predicted NO_x mixing ratios are also show for the sites where relatively complete NO_x observation data are available.

4.1 Resolution dependence of chemical processes

The difference between CBIV and SAPRC99 is further examined here by comparing both 81 km and 27 km predictions with hourly measurements data of EANET. The comparison of hourly O_3 predictions between CBIV and SAPRC99 shows an intriguing feature that with 81 km resolution CBIV performs better than SAPRC99, in reproducing the magnitude of observed O_3, but with 27 km resolution SAPRC99 shows better ability in capturing the observed 1-h maximum of O_3 mixing ratios, for example, 9–11 July at Sado-seki and some days at Ijira. In general the fine-grid predictions give better agreement against observations than the coarse-grid predictions for the minimum and maximum O_3 mixing ratios on observed low O_3 days. The average difference between the 81 km and 27 km simulations amounts to 40 ppb during these days. CMAQ 81 km calculations with both mechanisms tend to overpredict the maximum and minimum O_3 mixing ratios for observed low O_3 days at Sado-seki (2–8 July and 17–26 July) and at Oki (3–5 July). The overprediction of O_3 with 81 km resolution explains why the coarse grid simulations significantly overpredict monthly mean O_3 at Oki as presented in Fig. 2c.

Overall the fine-grid predictions give better agreement for the diurnal variations of

ACPD
8, 20239–20281, 2008

O_3 mixing ratios at most sites. In addition to better resolved precursors emissions and improved meteorological predictions with the high resolution, using hourly varying BCs instead of monthly mean values, might be another key reasons why the fine-grid simulation improves CMAQ performance in predicting O_3 variations. Increased spatial resolution improves results regardless of chemical mechanism. Our results going from hemispheric-scale (81 km) to regional scale (27 km) modeling grids, are consistent with Arnold and Dennis (2006) who show the similar improvement from regional (32 km) to urban (8 km and 2 km) scales. Since we are using global model BCs and then downscaling the 81 km results to 27 km, the results indicate the importance of the resolution-dependence of chemical processes in global-to-regional model downscaling.

The results suggest that the SAPRC99 mechanism may be used to predict high O_3 over urban areas but it requires high quality emission data for O_3 precursors, such as NO_x and the aggregated emissions for individual VOC species. The CBIV mechanism is more suitable for O_3 prediction at regional scales with a coarse grid spacing, i.e., 81 km in this study where emissions of O_3 precursors may have higher uncertainties.

4.2 Boundary layer evolution and NO_x titration

In addition to the chemical processes, the characterization of the near surface meteorology is needed to help interpret the differences between predicted and observed pollutant levels at ground-based measurement sites.

The temporal evolution of O_3 concentrations at the ground level is controlled strongly by the diurnal variation of the atmospheric boundary layer. We examine the correlations between temporal evolution of ground-level O_3 and boundary layer height at a rural site (Ijira-Fig. 10a) and two remote sites (Happo-Fig. 10b, Yusuhara-Fig. 10c). Observations at urban sites are directly influenced by on-site emissions which might not be well represented by 27 km model resolution, thus are not discussed in the present study.

In addition to O_3 and NO_x, Figs. 10a~10c also give the predicted boundary layer height (right/bottom axis) and wind speed at 10 m (left/top axis) from the 81 km and

ACPD
8, 20239–20281, 2008

27 km grid simulations of MM5.

4.2.1 Rural sites

Ijira is a rural EANET site located in the NO_x-rich central Japan. Intensified diurnal variations of NO_x and O_3 mixing ratios were observed at the Ijira site (Fig. 10a). All four simulations generally capture the observed obvious diurnal feature of O_3 mixing ratios at Ijira, yet tend to overpredict the observed lower than 20 ppb nighttime mixing ratios. The fine 27 km grid simulations of both CBIV and SAPRC99 significantly improve nighttime O_3 predictions as compared with measurements. Ozone at Ijira is formed and accumulated in the daytime boundary layer with observed concentration levels that reach the daily 1-h maximum of 120 ppb. The radiative cooling at night leads to the formation of the stable surface layer near the ground. Above the stable surface layer and under the upper-level inversion, the characteristics of the atmosphere are relatively uniform; this layer is called the nocturnal residual layer. If elevated NO emission sources such as tall industrial smokestacks are not present, O_3 concentrations in the residual layer remain high, since deposition and other removal processes that occur near the surface are absent aloft. This can be observed at the Mountain site Happo (Fig. 10b). At the rural site Ijira, however, relatively high concentration levels of NO_x were observed. Ozone concentrations at ground level at Ijira decrease after sunset to very low values at nighttime due to NO titration ($NO+O_3 \rightarrow NO_2+O_2$) and deposition processes and increase dramatically in the morning, reaching a maximum value in the afternoon (1–2 p.m. JST). The negative correlation between O_3 and NO_x suggests that O_3 formation at rural Ijira is in the VOC-limited regime.

The difference in nighttime O_3 concentration levels between fine and coarse simulations amounts to 40 ppb during 2–3 July and 21–23 July. During these periods the difference in nighttime boundary layer height is found to be ~500 m between the coarse and grid simulations of MM5 and explains why the find grid simulations of CMAQ predict lower nighttime O_3 concentrations. At the same time, however, NO_x mixing ratios during these days are overpredicted by the fine grid simulations. This is different from

ACPD
8, 20239–20281, 2008

9–11 July when the observed nighttime NO_x concentrations reach to 30 ppb and are well reproduced by the fine grid simulations. The artificial dilution of NO_x emissions in the coarse grid would partly explain overpredictions of nighttime O_3 during 9–11 July as a result of reduced NO titration.

We find that even with the 27-km fine resolution, CMAQ still largely overpredicts nighttime O_3 on several days and it is not influenced by choice of chemical mechanism. The overpredictions for nighttime O_3 are likely caused by a coarse vertical resolution for the first MM5 layer and vertical mixing physics. The 73-m depth of first MM5 layer may not be fine enough in simulating land surface interactions. We have tested CMAQ with a full range of 23 vertical layers from MM5 and the results do not improve nighttime O_3 overpredictions, suggesting that the vertical layer collapsing is not a primary reason for nighttime O_3 overprediction. In addition, nighttime boundary layer feature and associated vertical mixing play a key role on nighttime concentration level as discussed earlier. Furthermore, the minimum value of vertical eddy diffusivity (K_z) also has an important impact on nighttime concentrations (Zhang et al., 2006). Although CMAQ version 4.5.1 introduces a new option for minimum K_z allowing a larger value of minimum K_z for a larger fraction of urban land cover, the results presented here using the new K_z option suggest that more studies are needed for the vertical diffusion physics applied in the current version of CMAQ.

4.2.2 Remote sites

Different from the rural site Ijira, an obvious diurnal pattern of surface O_3 is not observed at Mt. Happo and Yusuhara, which are located in relatively clean remote areas. In remote areas outside the impact of urban pollutant plumes, the vertical mixing process might be the dominant mechanism for the buildup of ground-level O_3. All four simulations well capture the day-to-day variability in the observed data at Happo and Yusuhara. Although a similar diurnal pattern of boundary layer heights is shown at Ijira and Happo, nighttime O_3 at Mt. Happo remains high because elevated NO_x sources are not present. Daily variability of ground-level O_3 at Happo is shown to better cor-

ACPD
8, 20239–20281, 2008

relate (R=0.18) with changes of surface wind speed. High O_3 episodes during 7–10 July and 19–22 are correlated with low winds and stagnant conditions (slow moving high pressure system). The evolution of boundary layer at Yusuhara is quite different from that at Ijira and Happo. The boundary layer heights presented in Fig. 10c suggest that Yusuhara is in the relatively stable surface layer except during 9–11 July. During 9–11 July, a positive correlation of ground-level O_3 to boundary layer height is found at Yusuhara, indicating the influence of vertical transport of aloft pollutants into the surface layer. During 25–27 July, however, the dominance of photochemical production as indicated by high NO_x concentrations explains high concentration levels of surface O_3 in this period.

5 Conclusions

We have employed the CMAQ regional CTM at two horizontal scales (81 km and 27 km) to examine the mechanisms controlling surface ozone (O_3) in China and Japan, including the impacts of boundary conditions (BCs), photochemical production, regional transport, burning of agricultural residues over central east China, and meteorological conditions. Although measurement data for O_3 are relatively scarce in Asia, model predictions are compared with recently available monthly measurement data at six sites in China collected from research papers, and monthly and hourly data at nine sites in Japan provided by the EANET monitoring program.

The results show that wintertime surface O_3 over northern domain is most sensitive to the MOZART global BCs. Using measurement-adjusted O_3 BC improves CMAQ performance in reproducing the magnitude of observed O_3 at Mondy, Rishiri and Tappi, reducing the mean bias by ~5 ppb, while hourly varying BCs tends to improve the variation predictions. Ensemble mean of global multi-model predictions and data assimilation technique might be developed to reduce the uncertainty in global models, and enhance the coupling between regional and global models.

Summertime O_3 budgets over East Asia show complex interactions among regional

ACPD
8, 20239–20281, 2008

photochemical production involving anthropogenic and natural emissions, and East Asian summer monsoon circulation. For example, the O_3 budget in mid-latitudes early summer is dominated by the photochemical production involving precursor emissions of NMVOC and NO_x, whereas monsoonal intrusion of low-O_3 marine air masses from tropical Pacific plays a key role in controlling the O_3 budget in the boundary layer at lower latitudes of the Asian Pacific Rim. We find that the summer minimum of surface O_3 at two remote island sites (Hedo and Ogasawara) of south Japan and at two rural sites (Lin'an and Mt. Huang) of eastern China are well reproduced by the model. Over central east China, however, the simulated O_3 for 2001 does not exhibit the same sharp drop in July and August concentrations that is observed at two mountaintop sites (Tai and Hua) for 2004 and at Beijing for 1995–2005.

To help interpret the pronounced discrepancies of summertime O_3 between model simulations and measurements in central east China, we have examined the results of CMAQ with two widely used chemical schemes: CBIV and SAPRC99. The results suggest that there are high uncertainties in the photochemical production of summertime O_3 over the same region. The SAPRC99 mechanism produces higher values of mean summertime O_3 than the CBIV mechanism, amounting to a difference of 10 ppb, and explains why CMAQ with SAPRC99 tends to overpredict the observed O_3 over central east China and central Japan up to 25 ppb. CMAQ with the CBIV chemistry shows better performance in reproducing the monthly mean summertime minimum of observed O_3. Analysis of NCEP winds and geopotential heights demonstrates that the southwesterly monsoonal intrusion to central east China is weakened in August 2001 compared with the climatologically mean for 1980–2005. Further analysis of the diurnal cycle of O_3 mixing ratios at the Japanese sites shows that vertical mixing associated with boundary layer evolution has an important effect on the magnitude and temporal evolution of ground-level O_3. CMAQ with 81-km resolution tends to overpredict nighttime O_3 in urban and rural areas of East Asia. In terms of the uncertainty of precursors emissions, relatively strong densities of tropospheric NO_2 columns appear in June over central east China from the GOME instrument, while are not seen in the model-derived

ACPD
8, 20239–20281, 2008

values. MODIS fire count maps suggest that the lack of NO_x sources are likely due to the underestimated emissions from agricultural burning in central east China.

Improvements of regional CTMs will require the efforts in reducing the uncertainty in emissions, meteorology, photochemistry, and global pollution inflows, and in assimilating large-scale observational data. The characterization of meteorological conditions is needed to get a complete understanding of model performance, which poses a demand for establishing systematic measurements of both meteorological parameters and chemical tracers.

Acknowledgements. Meiyun Lin and Tracey Holloway were supported on this work by NASA Grant NNX07AL36G. The authors appreciate the EANET monitoring program for providing surface measurement data and Louisa Emmons at NCAR for providing the MODIS fire count data. We also thank Scott Spak and Eungle Lee at SAGE for constructive comments on the manuscripts.

References

Arnold, J. and Dennis, R. L.: Testing CMAQ chemistry sensitivities in base case and emissions control runs at SEARCH and SOS99 surface sites in the southeastern US, Atmos. Environ., 40, doi:10.1016/j.atmosenv.2005.05.055, 5027–5040, 2006. 20242, 20247, 20253, 20256

Byun, D. W.: A study of photochemical processes of the Houston-Galveston metropolitan airshed with EPA CMAQ, 2002 Models-3 User's Workshop, 21–23 October 2002, EPA, Research Triangle Park, NC, USA, 2002. 20248

Byun, D. W. and Ching, J. K. S. (Eds.): Science algorithms of the EPA models-3 community multi-scale air quality (CMAQ) modeling system, NERL, Research Triangle Park, NC, 1999. 20242

Byun, D. W. and Schere, K. L.: Review of the governing equations, computational algorithms, and other components of the Models-3 Community Multiscale Air Quality (CMAQ) modeling system, Appl. Mech. Rev., 59, 51–77, 2006. 20242

Carmichael, G. R., Ferm, M., Thongboonchoo, N., et al.: Measurements of sulfur dioxide, ozone and ammonia concentrations in Asia, Africa, and South America using passive samplers, doi:10.1016/S1352-2310(02)01009-9, Atmos. Environ., 37, pp. 1293–1308, 2003a. 20267

Carmichael, G. R., Tang, Y., Kurata, G., et al.: Regional-scale chemical transport modeling in support of the analysis of observations obtained during the TRACE-P experiment, J. Geophys. Res., 108, 8823, doi:10.1029/2002JD003117, 2003b. 20242
Carter, W.: Implementation of the SAPRC-99 Chemical Mechanism Into the MODELS-3 Framework, report to the United States Environmental Protection Agency, pp. 1–101, 29 January 2000. 20245
Ding, A. and Wang, T.: Influence of stratosphere-to-troposphere exchange on the seasonal cycle of surface ozone at Mount Waliguan in western China, Geophys. Res. Lett., 33, 1–4, doi:10.1029/2005GL024760, 2006. 20241
Ding, A. J., Wang, T., Thouret, V., Cammas, J.-P., and Nédélec, P.: Tropospheric ozone climatology over Beijing: analysis of aircraft data from the MOZAIC program, Atmos. Chem. Phys., 8, 1–13, 2008, http://www.atmos-chem-phys.net/8/1/2008/. 20241, 20251, 20252, 20253, 20267
EANET: Data Report on the Acid Deposition in the East Asian Region 2001, available at http://www.eanet.cc/product.html, Network Center for EANET, 2002. 20243, 20267
Faraji, M., Kimura, Y., McDonald-Buller, E., and Allen, D.: Comparison of the carbon bond and SAPRC photochemical mechanisms under conditions relevant to southeast Texas, Atmos. Environ., 42, 5821–5836, doi:10.1016/j.atmosenv.2007.07.048, 2008. 20247
Fiore, A. M., Jacob, D. J., Field, B. D., Streets, D. G., Fernandes, S. D., and Jang, C.: Linking ozone pollution and climate change: The case for controlling methane, Geophys. Res. Lett., 29, 25–1–25–4, doi:10.1029/2002GL015601, 2002. 20241
Fiore, A. M., Dentener, F., Wild, O., et al.: Muti-model estimates of intercontinental source-receptor relationships for ozone pollution, J. Geophys. Res., in press, 2008. 20251
Fishman, J., Ramanathan, V., Crutzen, P. J., and Liu, S. C.: Tropospheric ozone and climate, Nature, 818–820, 1979. 20241
Gery, M., Whitten, G. Z., Killus, J. P., and Dodge, M. C.: A Photochemical Kinetics Mechanism for Urban and Regional Scale Computer Modeling, J. Geophys. Res., 94, D10, 12 925–12 956, 1989. 20245
Glatthor, N., von Clarmann, T., Fischer, H., Funke, B., Grabowski, U., Höpfner, M., Kellmann, S., Linden, A., Milz, M., Steck, T., and Stiller, G. P.: Global peroxyacetyl nitrate (PAN) retrieval in the upper troposphere from limb emission spectra of the Michelson Interferometer for Passive Atmospheric Sounding (MIPAS), Atmos. Chem. Phys., 7, 2775–2787, 2007, http://www.atmos-chem-phys.net/7/2775/2007/. 20249

ACPD
8, 20239–20281, 2008

Grell, G. A., Dudhia, J., and Stauffer, D. R.: A description of the fifth-generation Penn State/NCAR mesoscale model (MM5), NCAR Tech. Note NCAR/TN-398+STR, 117 pp., 1994. 20244

Han, Z., Sakurai, T., Ueda, H., et al.: MICS-Asia II: Model intercomparison and evaluation of ozone and relevant species, Atmos. Environ., 42, 3491–3509, doi:10.1016/j.atmosenv.2007.07.031, 2007. 20242, 20251

Holloway T., Sakurai, T., Han, Z., et al.: MICS-Asia II: Impacts of global emissions on regional air quality in Asia, Atmos. Environ., 42, 3543–3561, doi:10.1016/j.atmosenv.2007.10.022, 2007. 20241, 20246

Hong, S.-Y. and Pan, H.-L.: Nonlocal boundary layer vertical diffusion in a medium-range forecast model, Mon. Weather Rev., 124, 2322–2339, 1996. 20244

Horowitz, L. W., Walters, S., Mauzerall, D. L., Emmons, L. K., Rasch, P. J., Granier, C., Tie, X. X., Lamarque, J. F., Schultz, M. G., Tyndall, G. S., Orlando, J. J., and Brasseur, G. P.: A global simulation of tropospheric ozone and related tracers: Description and evaluation of MOZART, version 2, J. Geophys. Res., 108, 4784, doi:10.1029/2002JD002853, 2003. 20242

Jacob, D. J.: Introduction to Atmospheric Chemistry, princeton University Press, Princeton, New Jersey, pp. 231–232, 1999. 20241

Kim, J., Lee, H., and Lee, S.: The characteristics of tropospheric ozone seasonality observed from ozone soundings at Pohang, Korea, Environ. Monit. Assess., 118, pp. 1–12, 2006. 20267

Lee, E., Chase, T. N., and Rajagopalan, B.: Seasonal forcasting of East Asian summer monsoon based on oceanic heat sources, Int. J. Climatol., 28, pp. 667–678, 2008. 20252

Li, J., Wang, Z., Akimoto, H., Gao, C., Pochanart, P., and Wang, X.: Modeling study of ozone seasonal cycle in lower troposphere over east Asia, J. Geophys. Res., 112, D22S25, doi:10.1029/2006JD008209, 2007. 20241, 20242, 20251, 20267

Lin, M., Oki, T., Bengtsson, M., Kanae, S., Holloway, T., and Streets, D. G.: Long-range transport of Acidifying substances in Asia – Part II: Source-receptor relationships, Atmos. Environ., 42, 5956–5967, doi:10.1016/j.atmosenv.2008.03.039, 2008a. 20244

Lin, M., Oki, T., Holloway, T., Streets, D. G., Bengtsson, M., and Kanae, S.: Long-range transport of acidifying substances in East Asia – Part I: Model evaluation and sensitivity studies, Atmos. Environ., 42, 5939–5955, doi:10.1016/j.atmosenv.2008.04.008, 2008b. 20243, 20244, 20245

Lin, W., Xu, X., Zhang, X., and Tang, J.: Contributions of pollutants from North China Plain to

surface ozone at the Shangdianzi GAW Station, Atmos. Chem. Phys., 8, 5889–5898, 2008c, http://www.atmos-chem-phys.net/8/5889/2008/. 20241, 20252, 20253, 20267

Liu, H. Y., Jacob, D. J., Chan, L. Y., Oltmans, S. J., Bey, I., Yantosca, R. M., Harris, J. M., Duncan, B. N., and Martin, R. V.: Sources of tropospheric ozone along the Asian Pacific Rim: An analysis of ozonesonde observations, J. Geophys. Res., 107, 4573, doi:10.1029/2001JD002005, 2002. 20241, 20250, 20252, 20255

Luecken, D. J., Phillips, S., Sarwar, G., and Jang, C.: Effects of using the CB05 vs. SAPRC99 vs. CB4 chemical mechanism on model predictions: Ozone and gas-phase photochemical precursor concentrations, Atmos. Environ., 42, doi:10.1016/j.atmosenv.2007.08.056, 2007. 20242, 20247

Ma, J., Zhou, X., and Hauglustaine, D.: Summertime tropospheric ozone over China simulated with a regional chemical transport model 2. Source contributions and budget, J. Geophys. Res., 107, 4612, doi:10.1029/2001JD001355, 2002. 20241

Ma, J., Zheng, X., and Xu, X.: Comment on "Why does surface ozone peak in summertime at Waliguan?" by Bin Zhu et al., Geophys. Res. Lett., 32, L01805, doi:10.1029/2004GL021683, 2005. 20241, 20267

Naja, M. and Akimoto, H.: Contribution of regional pollution and long-range transport to the Asia-Pacific region: Analysis of long-term ozonesonde data over Japan, J. Geophys. Res., 109, D21306, doi:10.1029/2004JD004687, 2004. 20241, 20250

Pochanart, P., Akimoto, H., Kajii, Y., Potemkin, V., and Khodzher, T.: Regional background ozone and carbon monoxide variations in remote Siberia/East Asia, J. Geophys. Res., 108, 4028, doi:10.1029/2001JD001412, 2003. 20267

Richter, A., Burrows, J. P., Nuss, H., Granier, C., and Niemeier, U.: Increase in tropospheric nitrogen dioxide over China observed from space, Nature, 437, 129–132, 2005. 20243

Sarwar, G., Luecken, D., Yarwood, G., Whitten, G., and Carter, W.: Impact of an updated Carbon Bond mechanism on predictions from the Community Multiscale Air Quality modeling system: preliminary assessment, J. Appl. Meteorol. Clim., 47, 3–14, doi:10.1175/2007JAMC1393.1, 2008. 20242

Streets, D. G., Bond, T. C., Carmichael, G. R., Fernandes, S. D., Fu, Q., He, D., Klimont, Z., Nelson, S. M., Tsai, N. Y., Wang, M. Q., Woo, J. H., and Yarber, K. F.: An inventory of gaseous and primary aerosol emissions in Asia in the year 2000, J. Geophys. Res., 108, 8809, doi:10.1029/2002JD003093, 2003. 20254

Tang Y., Carmichael, G. R., Thongboonchoo, N., et al.: Influence of lateral and top boundary

conditions on regional air quality prediction: A multiscale study coupling regional and global chemical transport models, J. Geophys. Res., 112, D10S18, doi:10.1029/2006JD007515, 2007. 20246

van der Werf, G. R., Randerson, J. T., Giglio, L., Collatz, G. J., Kasibhatla, P. S., and Arellano, A. F.: Interannual variability in global biomass burning emissions from 1997 to 2004, Atmos. Chem. Phys., 6, 3423–3441, 2006, http://www.atmos-chem-phys.net/6/3423/2006/. 20254

Wang, T., Cheung, V. T. F., Anson, M., and Li, Y. S.: Ozone and related gaseous pollutants in the boundary layer of eastern China: Overview of the recent measurements at a rural site, Geophys. Res. Lett., 28, 2372–2376, 2001. 20267

Wang, T., Ding, A., Gao, J., and Wu, W. S.: Strong ozone production in urban plumes from Beijing, China, Geophys. Res. Lett., 33, 1–5, doi:10.1029/2006GL027689, 2006a. 20251, 20253, 20267

Wang, Z., Li, J., Wang, X., Pochanart, P., and Akimoto, H.: Modeling of regional high ozone episode observed at two mountain sites (Mt. Tai and Huang) in east China, J. Atmos. Chem., 55, 253–272, 2006b. 20242

Wild, O., Prather, M. J., Akimoto, H., Sundet, J. K., Isaksen, I. S. A., Crawford, J. H., Davis, D. D., Avery, M. A., Kondo, Y., Sachse, G. W., and Sandholm, S. T.: Chemical transport model ozone simulations for spring 2001 over the western Pacific: Regional ozone production and its global impacts, J. Geophys. Res., 109, 1–14, doi:10.1029/2003JD004041, 2004. 20241

Xu, X., Lin, W., Wang, T., Yan, P., Tang, J., Meng, Z., and Wang, Y.: Long-term trend of surface ozone at a regional background station in eastern China 1991–2006: enhanced variability, Atmos. Chem. Phys., 8, 2595–2607, 2008, http://www.atmos-chem-phys.net/8/2595/2008/. 20241

Yamaji, K., Ohara, T., Uno, I., Tanimoto, H., Kurokawa, J., and Akimoto, H.: Analysis of the seasonal variation of ozone in the boundary layer in East Asia using the Community Multi-scale Air Quality model: What controls surface ozone levels over Japan?, Atmos. Environ., 40, 1856–1868, 2006. 20242, 20255

Yarwood, G., Stoeckenius, T. E., Heiken, J. G., and Dunker, A. M.: Modeling weekday/weekend ozone differences in the Los Angeles region for 1997, J. Air Waste Manage., 53, 864–875, 2003. 20248

Zhang, Y., Liu, P., Queen, A., Misenis, C., Pun, B., Seigneur, C., and Wu, S. Y.: A comprehensive performance evaluation of MM5-CMAQ for the Summer 1999 Southern Oxidants Study episode- Part II: Gas and aerosol predictions, Atmos. Environ., 40, 4839–4855, 2006.

20253, 20258
Zhang, M. G., Uno, I., Carmichael, G. R., et al.: Large-scale structure of trace gas and aerosol distributions over the western Pacific Ocean during the Transport and Chemical Evolution Over the Pacific (TRACE-P) experiment, J. Geophys. Res., 108, doi:10.1029/2002JD002946, 2003. 20242
Zhu, B., Akimoto, H., Wang, Z., Sudo, K., Tang, J., and Uno, I.: Why does surface ozone peak in summertime at Waliguan?, Geophys. Res. Lett., 31, 1–4, doi:10.1029/2004GL020609, 2004. 20241

Table 1. Measurement data used in this study.

Name	Type	LAT	LONG	HT (m a.s.l.)	Periods	References
Mondy	Remote	51.67	101.00	2000	1997–1999	Pochanart et al. (2003)
Mt. Waliguan	Mountain	36.28	100.90	3810	1994–2003	Ma et al. (2005)
Beijing	Urban	39~42	115.5~118.5	600	1995–2005	Ding et al. (2008)
Beijing	Urban	40.35	116.30	280	Jun–Jul 2005	Wang et al. (2006a)
Shangdianzi	Rural	40.65	116.12	294	2004–2006	Lin et al. (2008c)
Mt. Hua	Mountain	34.49	110.09	2064	2004–2005	Li et al. (2007)
Mt. Tai	Mountain	36.25	117.10	1533	2004–2005	Li et al. (2007)
Mt. Huang	Mountain	30.13	118.15	1836	2004–2005	Li et al. (2007)
LinAn	Rural	30.30	119.73	132	1999–2000	Wang et al. (2001)
Pohang	Remote	36.00	129.00	–	1995–2000	Kim et al. (2006)
Rishiri	Remote	45.12	141.23	40	2001	EANET (2002)
Tappi	Remote	41.25	141.35	105	2001	EANET (2002)
Sado-seki	Remote	38.25	138.40	110	2001	EANET (2002)
Happo	Remote	36.68	137.80	1850	2001	EANET (2002)
Ijira	Rural	35.57	136.70	140	2001	EANET (2002)
Oki	Remote	36.28	133.18	90	2001	EANET (2002)
Yusuhara	Remote	32.73	132.98	225	2001	EANET (2002)
Hedo	Remote	26.78	128.23	50	2001	EANET (2002)
Ogasawara	Remote	27.08	142.22	230	2001	EANET (2002)
Mt. Sto. Tomas	Mountain	16.00	120.00	2200	1999–2000	Carmichael et al. (2003a)
Bhubeneswar	Remote	20.25	85.87	24	1999–2001	Carmichael et al. (2003a)
ChiangMai	Remote	20.08	99.38	807	1999–2000	Carmichael et al. (2003a)

ACPD
8, 20239–20281, 2008

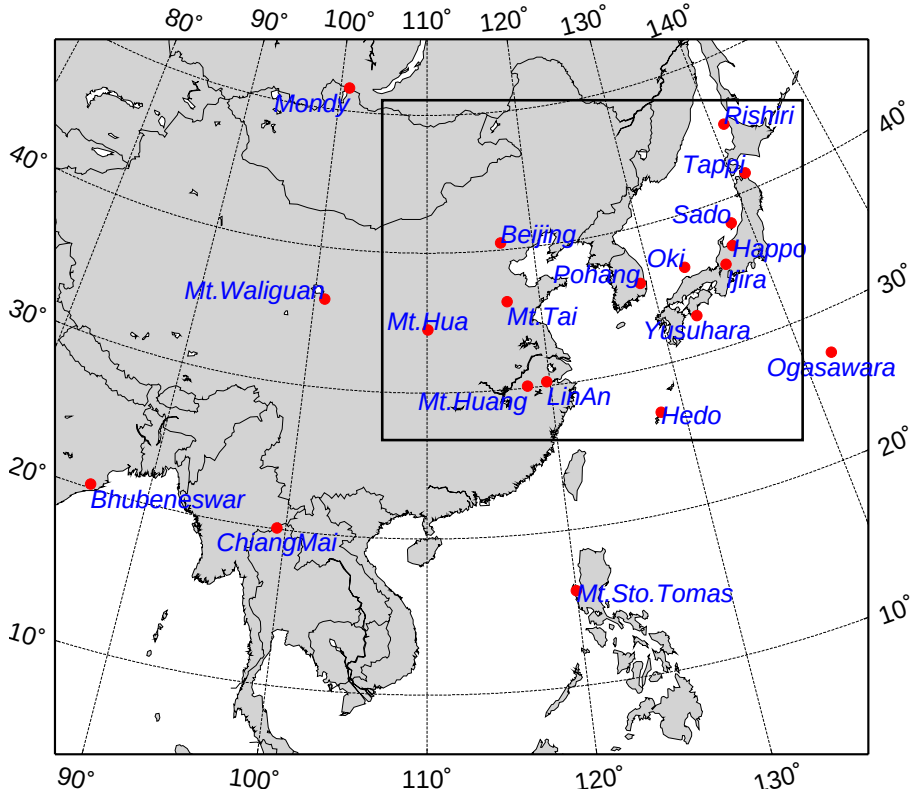

Fig. 1. Model domains (outer region for 81×81 km^2 and inner region for 27×27 km^2) and ground-based measurement sites

ACPD
8, 20239–20281, 2008

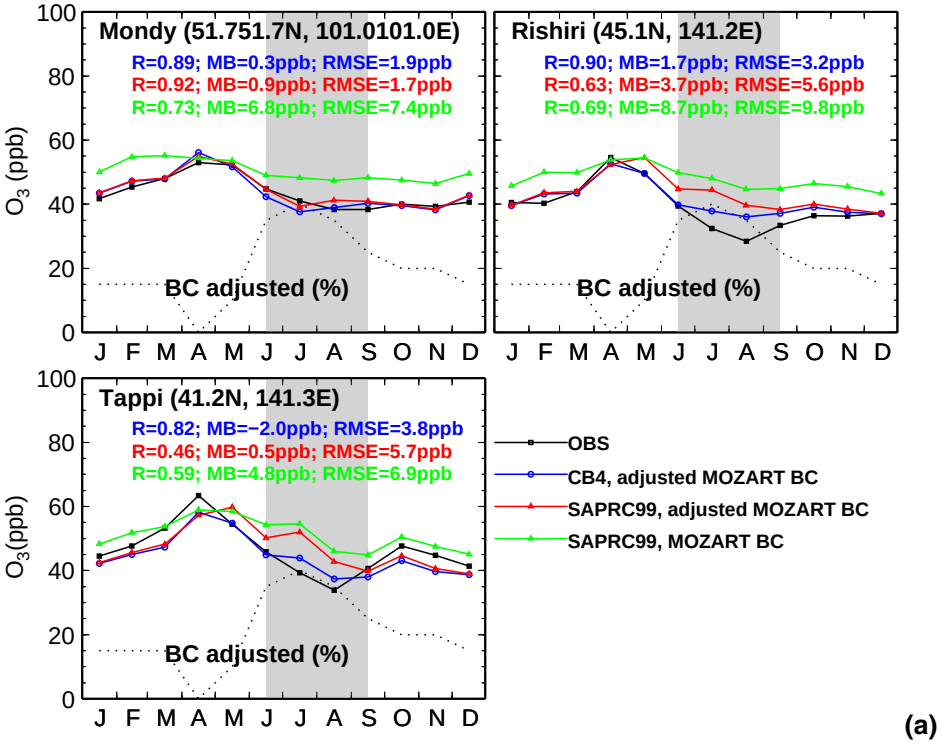

Fig. 2a. Seasonal variations of observed and predicted surface ozone at the measurement site at **(a)** high latitudes, **(b)** low latitudes, and **(c)** middle latitudes. Summer months are marked as gray. The dotted line shows the percentage adjustments of O_3 concentrations imported from the MOZART global model at the domain boundaries. The adjusted percentage is correspondent to the bias between MOZART predictions and measurements over Japan. The whiskers are 1 standard deviation of measurement data.

ACPD
8, 20239–20281, 2008

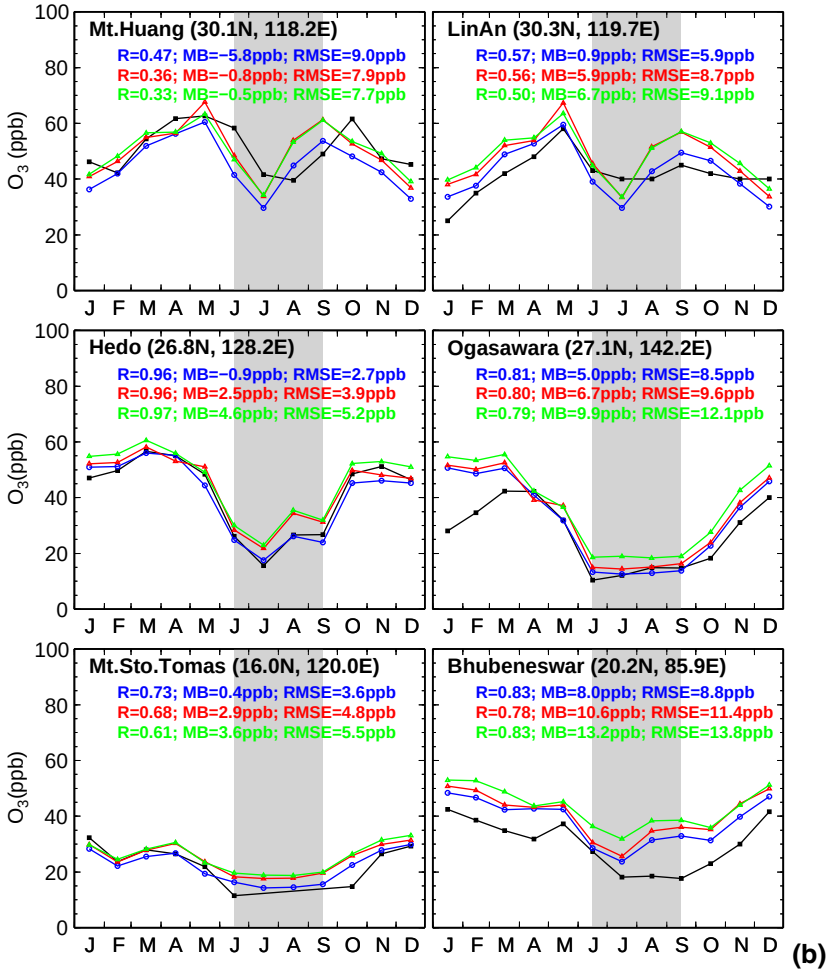

Fig. 2b. Continued.

ACPD
8, 20239–20281, 2008

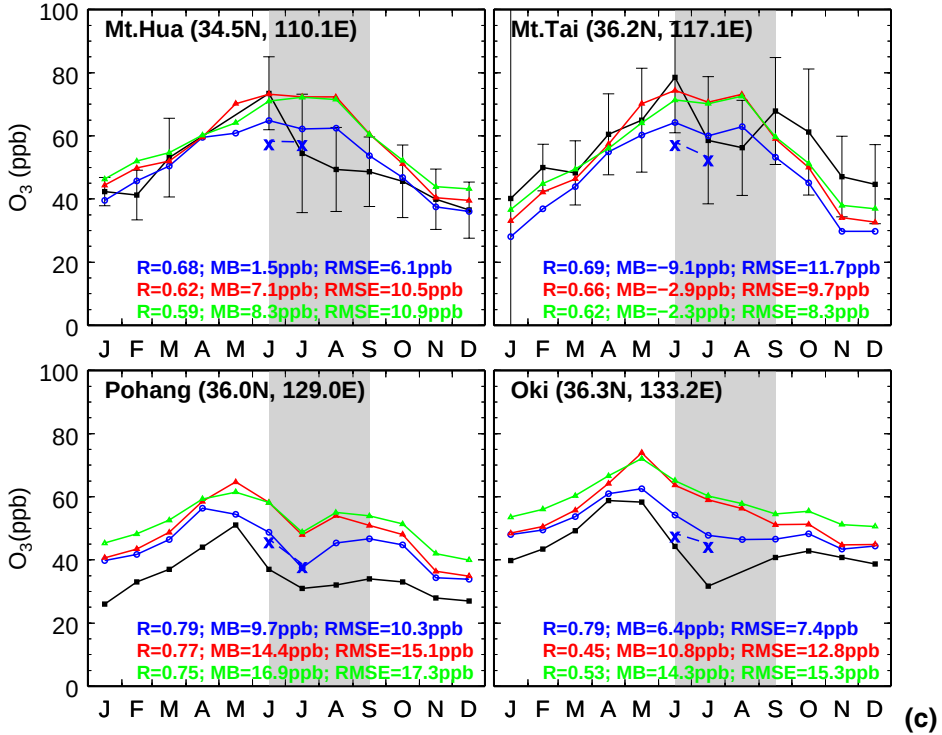

Fig. 2c. Continued. The blue cross for June and July show the CBIV predictions with 27-km resolution.

ACPD
8, 20239–20281, 2008

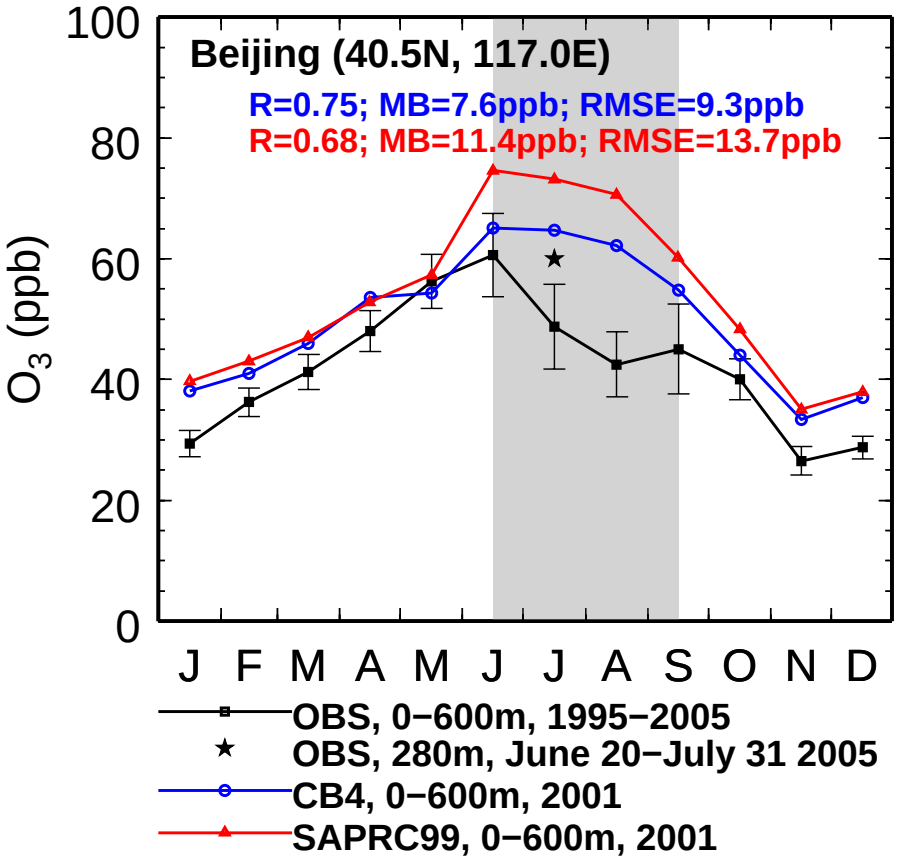

Fig. 3. Observed and simulated seasonal cycle of O_3 in the lower troposphere over Beijing. The whiskers are 1 standard deviation of measurement data.

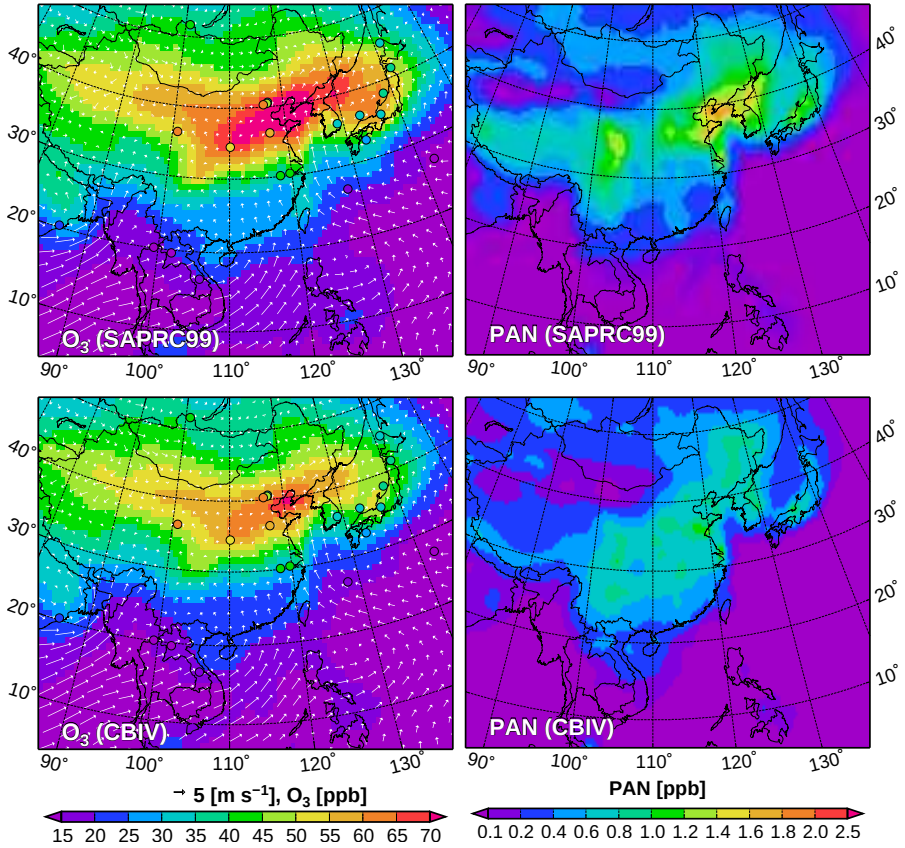

Fig. 4. Distributions of monthly mean surface O_3 and PAN in July 2001 from the SAPRC99 (upper panel) and CBIV (lower panel) simulations. The filled circles show the observed values of O_3 at EANET sites in Japan and other sites reported in recent publications as denoted in Table 1. The wind vectors at near surface from MM5 are also shown.

ACPD
8, 20239–20281, 2008

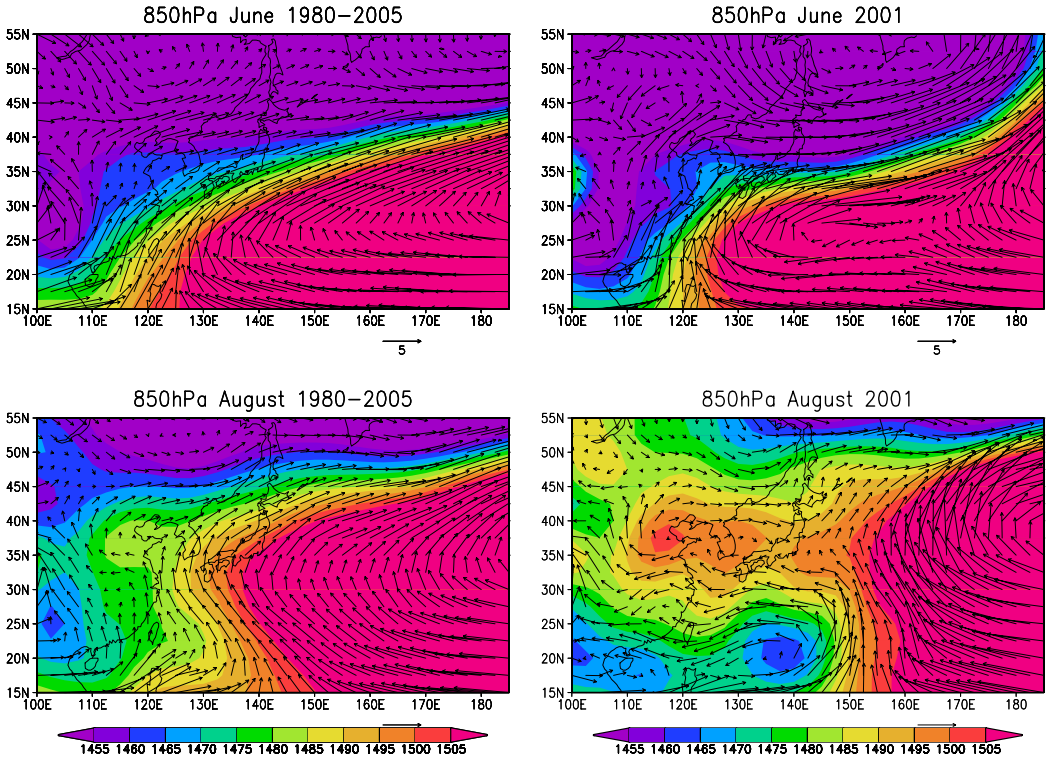

Fig. 5. Monthly mean wind vectors (m/s) and geopotential heights (gpm) at 850 hPa in June and August for climatological mean during 1980–2005 and for 2001.

ACPD
8, 20239–20281, 2008

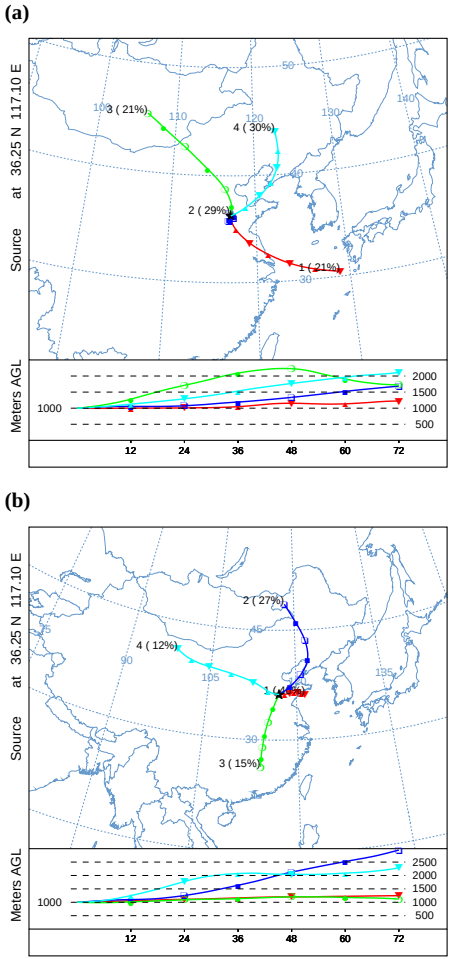

Fig. 6. Clusters of three-day back trajectories ending at Mt. Tai during **(a)** August 2001 and **(b)** August 2004.

ACPD
8, 20239–20281, 2008

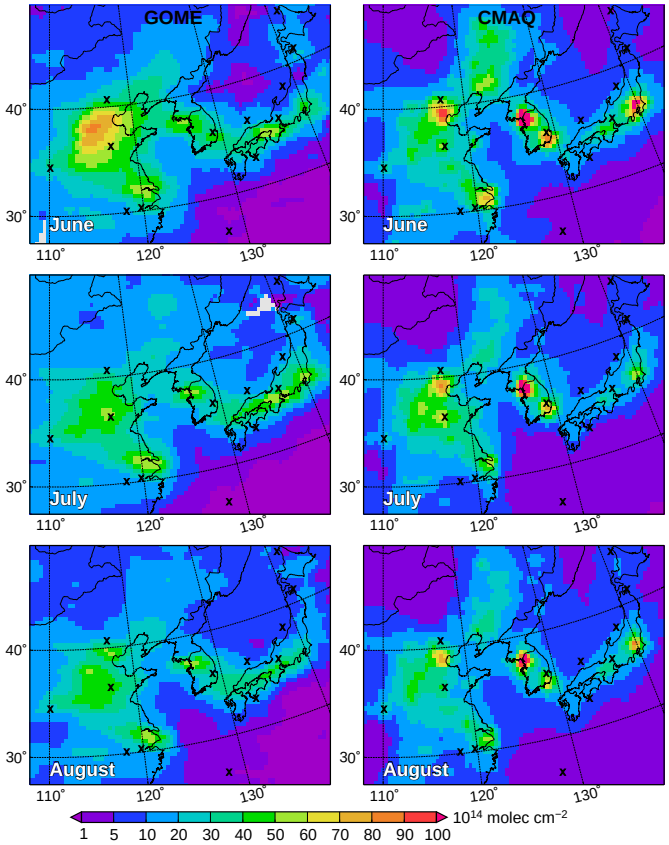

Fig. 7. Satellite measurements of tropospheric NO_2 column from GOME (left panel) and the calculated values from CMAQ (right panel) at the ERS-2 overpass time for June, July and August of 2001. The crosses indicate the locations of measurement sites shown in Figs. 2 and 3.

ACPD
8, 20239–20281, 2008

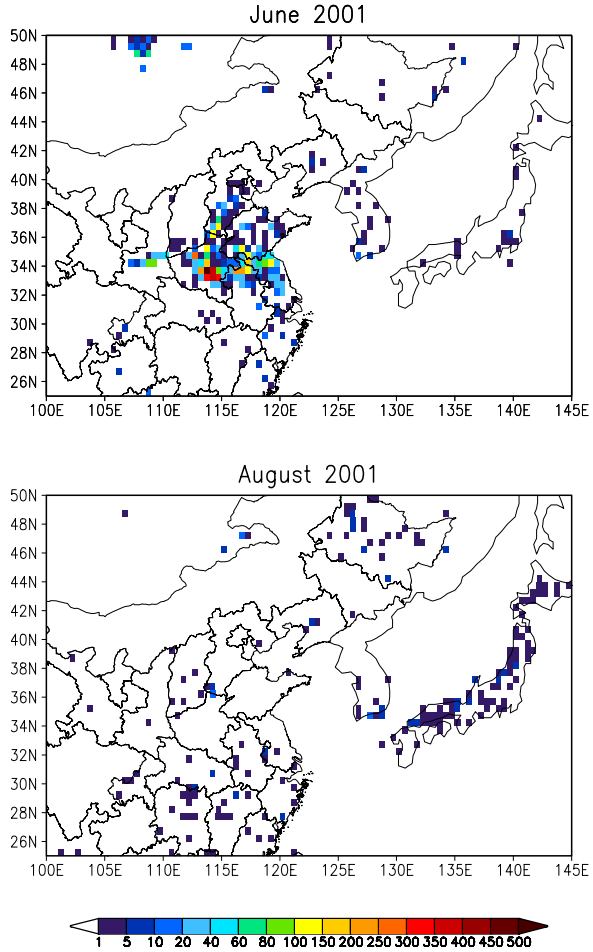

Fig. 8. MODIS total fire count in June and August 2001.

ACPD

8, 20239–20281, 2008

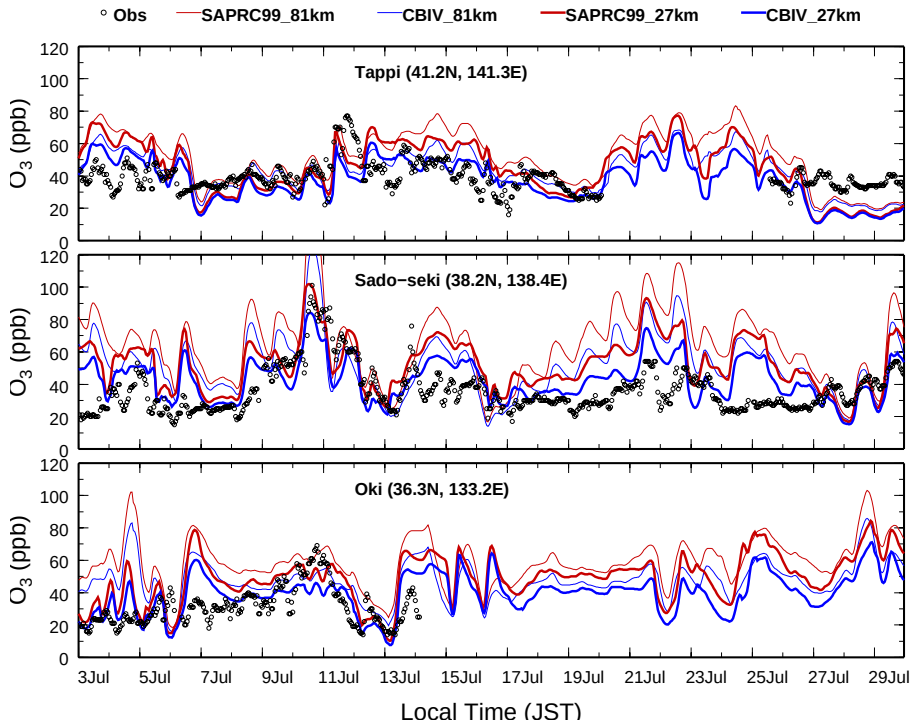

Fig. 9. Hourly time series of observed and predicted mixing ratios of O_3 at Tappi, Sado-seki, and Oki in July 2001.

ACPD
8, 20239–20281, 2008

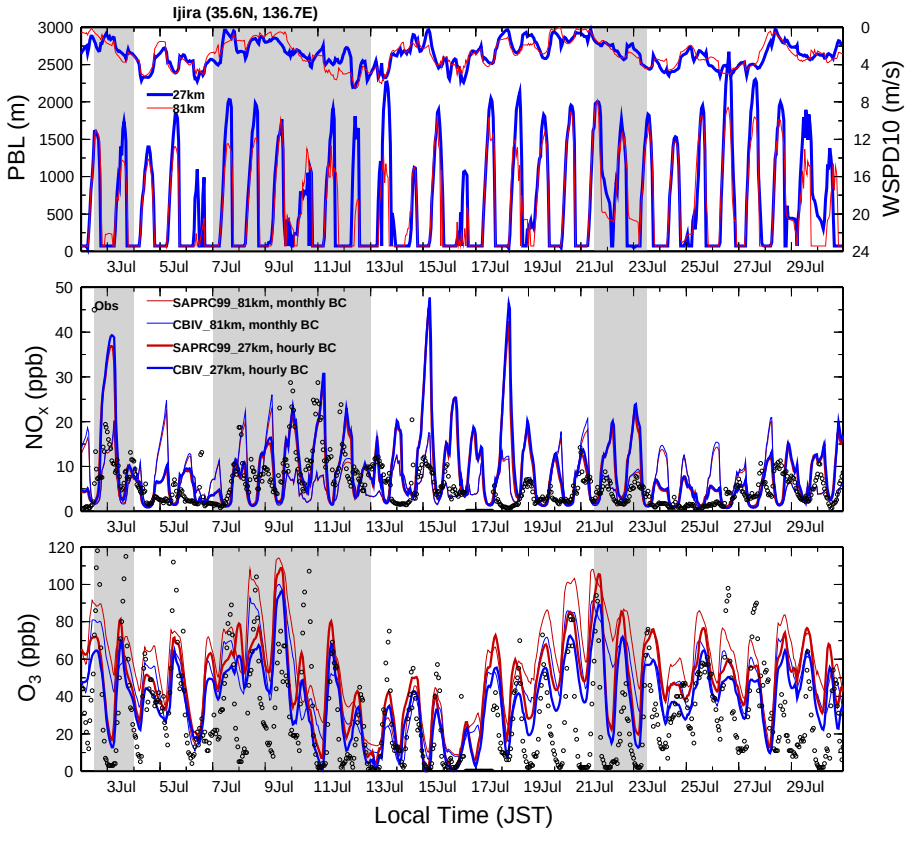

Fig. 10a. Hourly time series of observed and predicted mixing ratios of NO_x and O_3 in July 2001 **(a)** at the rural site Ijira, **(b)** the remote mountain site Happo, and **(c)** the remote site Yusuhara. The upper panel shows MM5 predicted boundary layer heights (left/bottom axis) and wind-speed at 10 m (right/top axis). Specific days with large difference among predictions are marked as gray.

ACPD
8, 20239–20281, 2008

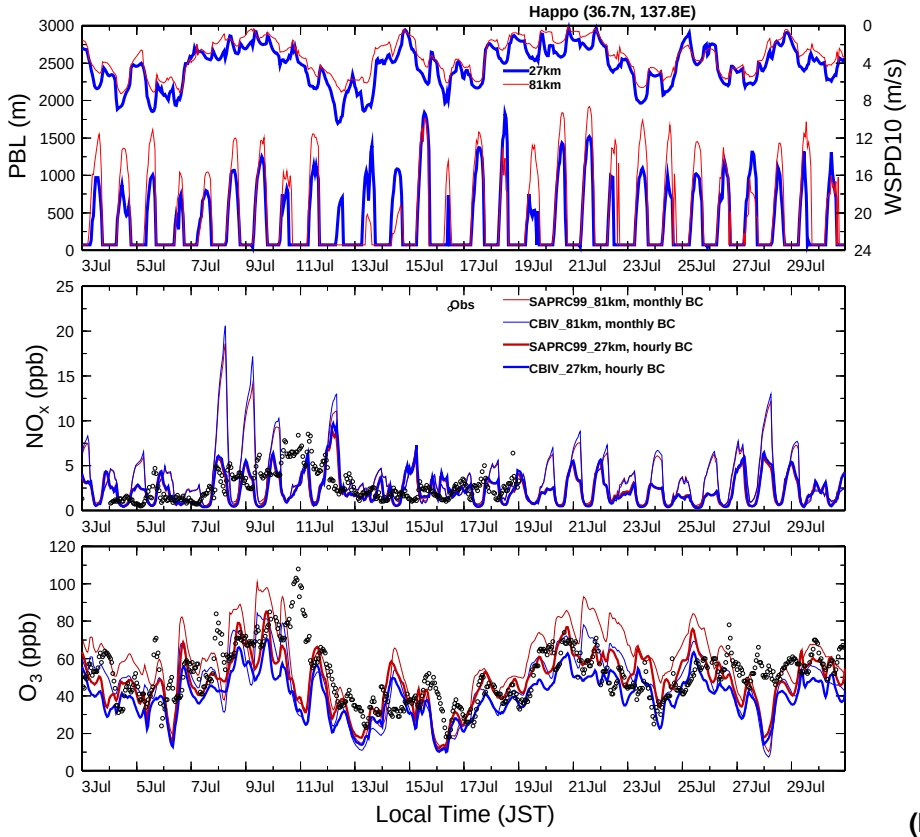

(b)

Fig. 10b. Continued.

ACPD
8, 20239–20281, 2008

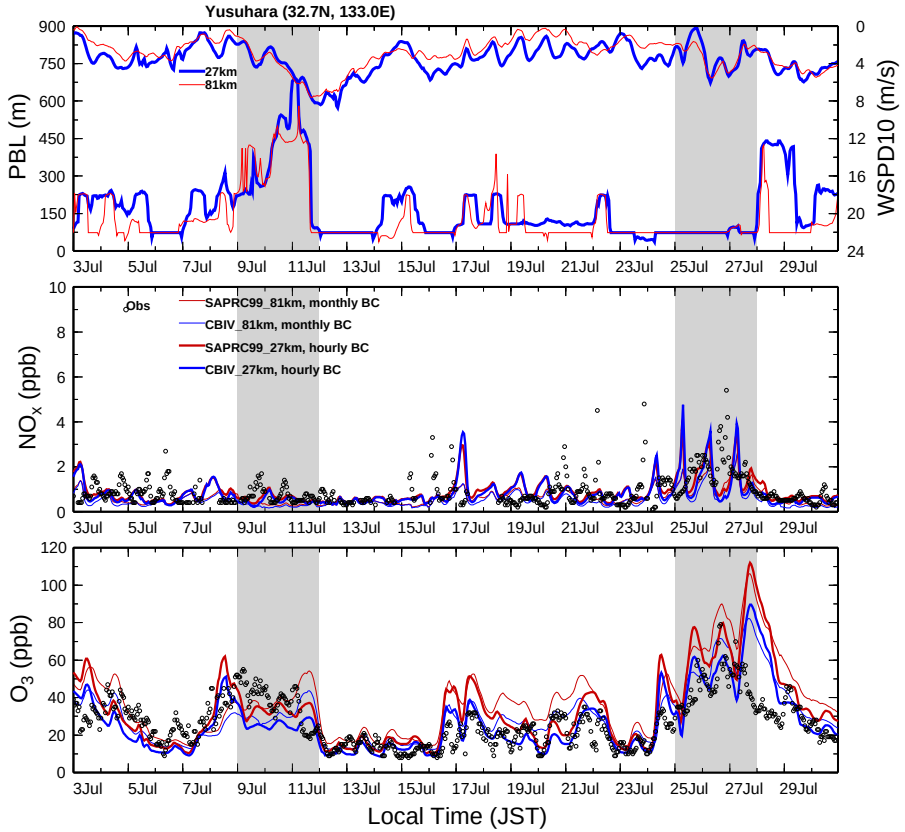

(c)

Fig. 10c. Continued.

ACPD
8, 20239–20281, 2008